Estimating the Sensitivity of Mechanosensitive Ion Channels to Membrane Strain and Tension

Guillaume T. Charras,* Beatrice A. Williams,† Stephen M. Sims,† and Mike A. Horton*
*Bone and Mineral Centre, Department of Medicine, University College London, London, United Kingdom; and †Canadian Institutes of Health Research Group in Skeletal Development and Remodeling, Department of Physiology and Pharmacology, The University of Western Ontario, London, Ontario, Canada

ABSTRACT Bone adapts to its environment by a process in which osteoblasts and osteocytes sense applied mechanical strain. One possible pathway for the detection of strain involves mechanosensitive channels and we sought to determine their sensitivity to membrane strain and tension. We used a combination of experimental and computational modeling techniques to gain new insights into cell mechanics and the regulation of mechanosensitive channels. Using patch-clamp electrophysiology combined with video microscopy, we recorded simultaneously the evolution of membrane extensions into the micropipette, applied pressure, and membrane currents. Nonselective mechanosensitive cation channels with a conductance of 15 pS were observed. Bleb aspiration into the micropipette was simulated using finite element models incorporating the cytoplasm, the actin cortex, the plasma membrane, cellular stiffening in response to strain, and adhesion between the membrane and the micropipette. Using this model, we examine the relative importance of the different cellular components in resisting suction into the pipette and estimate the membrane strains and tensions needed to open mechanosensitive channels. Radial membrane strains of 800% and tensions of 5 10^{-4} N.m^{-1} were needed to open 50% of mechanosensitive channels. We discuss the relevance of these results in the understanding of cellular reactions to mechanical strain and bone physiology.

INTRODUCTION

Bone is a tissue that adapts to mechanical stimuli in a process driven by cells of the osteoblastic lineage, the bone-forming osteoblasts, and the osteocytes. However, due to the complex microarchitecture of bone matrix, the exact strain magnitude to which osteoblasts and osteocytes are exposed in vivo is unknown. Knowledge of the sensitivity of osteoblasts to mechanical strain is of great importance for the understanding of the detection and adaptation of bone to its mechanical environment and in identifying new drugs designed to stimulate bone formation through a shift in this sensitivity. Recently, we used atomic force microscopy (AFM) to mechanically stimulate osteoblasts (Charras and Horton, 2002). We showed that the strain magnitude for which half of the cells reacted ($\varepsilon = 2.5\%$) with an increase in cytosolic calcium concentration was ~10-fold higher than strain magnitudes measured by strain gauges on the bone surface of mammals during a variety of activities ($\varepsilon \approx 0.3\%$; Rubin and Lanyon, 1984). In our prior studies using AFM to mechanically stimulate osteoblasts, the response to initial membrane deformation involved stretch-activated cation channels and was sensitive to surface tensile strains (Charras and Horton, 2002). Therefore, we sought to examine the sensitivity to mechanical strain of this step more in detail.

Stretch-activated cation channels were originally discovered by Guharay and Sachs (1984). They have since then been reported in a variety of cell types including osteoblastic cell lines (Davidson et al., 1990; Duncan and Misler, 1989; for a review, see Sachs and Morris, 1998) and their crystal structure has been elucidated in prokaryotes (Chang et al., 1998; Sukharev et al., 2001). Several groups have shown that mechanosensitive channel openings elicited by micropipette aspiration could give rise to whole cell cytosolic calcium responses, thereby reinforcing the putative role of mechanosensitive channels as the first step in the transduction of external physiological mechanical stimuli into whole cell responses (Kirber et al., 2000; Zou et al., 2002).

One of the established methods of estimating cellular elasticity relies on the aspiration of a bleb of cellular membrane into a micropipette in conjunction with video microscopy recording (Evans et al., 1976; Jones et al., 1999; Theret et al., 1988). These experiments, combined with a theoretical model of the mechanics of bleb formation, enable the relevant mechanical parameters to be estimated. To date, two different mechanical models have been applied to cells, and either one allows the simulation of cellular deformations in response to micropipette aspiration. One describes cells as having a solid cortex and viscous liquid core and has been used to model the aspiration of cells with no or little cytoskeleton (such as red blood cells or unattached leukocytes) into micropipettes (Discher et al., 1998; Drury and Dembo, 1999). The other describes cells spread on a substrate with a well developed cytoskeleton as being elastic solids, and has been applied to the aspiration of cells into micropipettes (Theret et al., 1988) or to micro-

Submitted January 20, 2004, and accepted for publication July 26, 2004.

Guillaume T. Charras and Beatrice A. Williams contributed equally to this work.

Address reprint requests to Dr. Guillaume Charras, Harvard Medical School, SGM 604, 250 Longwood Ave., Boston, MA 02130. Tel.: 617-432-3724; Fax: 617-432-3702; E-mail: gcharras@hms.harvard.edu.

0006-3495/04/10/2870/15 $2.00

doi: 10.1529/biophysj.104.040436

indentation experiments and full cell stimulation (Charras and Horton, 2002; Radmacher, 1997). Moreover, cell aspiration into micropipettes can be combined with single-channel patch-clamp electrophysiology. Using such a combination, Sukharev et al. (1999) related the membrane tension to the open probability of the prokaryotic stretch-activated channel, MscL, reconstituted in artificial lipid bilayers.

In this study, we determined whether primary osteoblasts possessed stretch-activated cation channels and estimated the membrane strain and tension necessary to activate these channels. To achieve this, we used a combination of experimental and modeling techniques to estimate the strain and tension needed to open stretch-activated channels. Simultaneous patch-clamp electrophysiology, video microscopy, and pressure recordings enabled us to acquire experimental curves relating membrane extension into the micropipette and the opening of stretch-activated channels in response to the aspiration pressure. We report the presence of nonselective stretch-activated cation channels with a conductance of 15 pS in primary osteoblasts. Finite element (FE) modeling was used to simulate the aspiration process. When linear stiffening with strain was incorporated into the model, we were able to simulate the experimental aspiration curves and estimated that membrane strains of 800% and membrane tensions of 5 10^{-4} $N.m^{-1}$ were needed for the mechanosensitive channels present in the patch to be open 50% of the time. We examined the influences of relevant mechanical parameters on the strain elicited in the cell by micropipette aspiration and showed that the micropipette inner diameter and opening angle have no effect on the strain magnitude elicited, whereas cytoplasmic Poisson ratio and elasticity, and cortical elasticity do. Finally, we discuss the biological and mechanical sources of the large discrepancy between the estimates of the strain needed to open mechanosensitive channels obtained from AFM and micropipette aspiration experiments. These two strain estimates may be compatible given the excess membrane present in all cells and the plastic deformations induced in the cells due to micropipette aspiration. Furthermore, these results may be reconciled if membrane tension is the gating stimulus in mechanosensitive channels. Our study points toward a need for an in depth biophysical examination of the cell membrane and subplasmalemmal cytoskeleton in living cells.

METHODS

Cell culture

All procedures involving animals were approved by the Council on Animal Care at the University of Western Ontario and complied with the guidelines of the Canadian Council on Animal Care. Procedures involving animals at the University College London complied with United Kingdom Schedule 1 guidelines. Osteoblasts were isolated from the long bones of neonatal rats by mechanical disaggregation and cultured on glass coverslips for 48 or 72 h at 37°C in an atmosphere of 5% CO_2 in air in Dulbecco's modified Eagle's medium (Gibco Life Technologies, Paisley, UK) supplemented with 10% fetal calf serum, 2% glutamine, and 2% penicillin-streptomycin.

Patch-clamp recordings

For recording currents across the cell membrane, we used conventional cell-attached patch configuration. For most experiments, the electrode solution contained 135 mM KCl, 20 mM HEPES, 10 mM glucose, 1 mM $MgCl_2$, 1 mM $CaCl_2$, pH = 7.4. Cells were superfused (1–2 $ml.min^{-1}$) with a standard extracellular solution containing 130 mM NaCl, 5 mM KCl, 20 mM HEPES, 10 mM glucose, 1 mM $CaCl_2$, 1 mM $MgCl_2$, pH = 7.4. To test whether the mechanosensitive channels conducted Cl^-, aspartate was substituted for Cl^- in the electrode solution. To test whether the channels were mechanosensitive, the nonspecific mechanosensitive channel blocker Gd^{3+} (50 μM) was added to the electrode solution (Sachs and Morris, 1998). To serve as a positive control, an equal number of cells from the same culture were also analyzed without Gd^{3+} in the electrode solution on the same day. To test whether the channels were nonselective for monovalent cations, the electrode and perfusion solutions were inverted in some experiments. In other studies, KCl in the electrode solution was substituted by NaCl isotonically to give a solution containing 65mM NaCl, the cells being superfused with the standard extracellular bathing solution.

Pipettes were made from borosilicate glass (inner diameter 1.1 mm, outer diameter 1.5 mm, Sutter, Novato, CA) on a Flaming Brown Micropipette puller (Sutter), were fire-polished and coated with bees wax to reduce noise. The pipette resistance varied between 4 and 8 MΩ. Gigaohm seals were obtained by approaching the pipette toward the cell and applying a light suction onto the membrane and slowly changing the holding potential from 0 to −40 mV. We sought to work only with ''gentle'' patches (Sachs and Morris, 1998) and, as a consequence, seals obtained with suction pressures >10 mm Hg were discarded, as were those displaying spontaneous channel activity. Once a gigaseal had formed, the pressure and the holding potential were returned to zero. All currents were recorded at room temperature (21–25°C) with an Axopatch 1D (Axon Instruments, Union City, CA), filtered at 500 Hz or 1 kHz, and sampled at 5 kHz with a Digidata 1320A (Axon Instruments), and pCLAMP 8 software (Axon Instruments). No holding potential was applied onto the patch so that recording conditions were as close as possible to physiological conditions. Data for I/V curves were acquired by varying the patch potential when the channels were open and examining the changes in the current amplitude.

Mechanical stimulus and pressure measurement

Step changes in suction pressure were applied to the patches to stimulate channel opening. The pressure circuit consisted of the micropipette, a valve to isolate the pipette from the rest of the circuit, the pressure transducer (model P1000B, Narco Biosystems, Austin, TX) and a three-way valve to link a syringe to the circuit (Fig. 3 *C*). Quick changes in pressure were achieved by isolating the pipette from the rest of the circuit and adjusting the pressure in the circuit to the desired value. Pressure drop when the micropipette was reconnected to the rest of the circuit was minimal. Patch pressure was recorded simultaneously with the membrane currents using the pCLAMP software. Pressure was applied in 30 s periods. It was then released and 30 s later another pressure increment was applied. This was continued until the membrane ruptured or the seal was lost. The pressure was increased in 20 mm Hg increments. All pressures are given in pascals consistent with the Système international d'unités used in the FE simulations (1 mm Hg = 0.133 kPa).

Imaging and video microscopy

The cells and patch pipette were imaged during pressure application on a Nikon inverted microscope using Hoffman modulation optics and a 40× objective (numerical aperture = 0.5). VHS video recordings were obtained using a time-lapse video recorder (AG-6720, Panasonic, Secaucus, NJ) connected to a video camera (AVC-D5, Sony, Tokyo, Japan) mounted on the side port of the microscope. They were subsequently examined and

digitized using a frame grabber (Optimas 3.1, Bioscan, Washington, DC). Finally, the movies were postprocessed using a custom-written application under Pv-Wave (Visual Numerics, Boulder, CO) running on an SGI O_2 workstation (SGI, Mountain View, CA) to yield time-averaged images of the pipette and the membrane bleb. The images were the time average of 10 video images and were taken 5 s after the pressure had been changed to ensure that the bleb was stationary. The images were calibrated using a graticule.

Bleb height measurement

An application running under Pv-Wave was written to measure the bleb extension within the micropipette. Digitized time-averaged videos were imported into the program. The videos had one image per pressure change. The first step was to position a cursor at the entry of the pipette. On each subsequent image, a second cursor was positioned at the center part of the apex of the membrane extension. The program then calculated the distances between the two cursors (in micrometers) for each time point, corrected for the pipette angle to the horizontal and output the results to a file which was then imported into Excel (Microsoft, Redmond, WA).

Twelve experiments giving the bleb height as a function of pressure applied were grouped together by averaging to yield a ''representative experiment''. This representative experiment was then simulated using FE modeling.

Electrophysiology data analysis

Current records were analyzed with pClamp 6.0 (Axon Instruments) to obtain channel amplitudes and open probabilities P_{open}. The open probabilities were obtained assuming that all of the stretch-activated channels present in the patch had been observed during the experiment (in line with Hase et al., 1995; Sukharev et al., 1999). Graphs giving P_{open} as a function of the applied pressure were generated and a sigmoid curve was fitted to the data (Sachs and Morris, 1998) using KaleidaGraph (Synergy Software, Essex Junction, VT).

The average pressure at which the first mechanosensitive channel opening was detected was calculated from 38 experiments, each on a different cell. Pipette potentials were converted to membrane potentials assuming a resting membrane potential of −40 mV (Dixon et al., 1984). Weighted linear functions were fitted to the average data from each electrode solution using KaleidaGraph software. Possible differences in mechanosensitivity due to the age of the culture (48 h or 72 h), the solution present in the electrode, or the presence or absence of gadolinium in the electrode solution were examined using a chi-square test. The results were deemed significant if $p < 0.05$.

Finite element modeling

An FE model of the membrane aspiration process was generated to simulate the ''representative experiment'' (Fig. 4). By computing the bleb height for the experimentally derived pressures of activation of the mechanosensitive channels, we estimated the membrane strain and tension needed to elicit mechanosensitive channel openings. As the cells were strongly adherent to the substrate and had a well-developed cytoskeleton, we modeled the cell as a linear elastic solid (Zhu et al., 2000) rather than a viscous fluid surrounded by a solid core (as for red blood cells or leukocytes in suspension, Discher et al., 1998; Drury and Dembo, 1999). Regions undergoing plastic deformation could be identified knowing the plastic transition strain (evaluated for spread cells in Appendix II). The viscoelastic properties of the cell were ignored because only equilibrium positions of the cell membrane were recorded in the experimental data. Because the cell cortex and plasma membrane play an important role in the resistance to aspiration, these together with adhesion between the plasma membrane and the micropipette were incorporated into the model. To simplify modeling, the cell membrane was modeled as a thin solid shell rather than a viscous fluid. All FE calculations were carried out with CAST3M, a general purpose FE solver with an integrated pre- and postprocessor (CAST3M, Commissariat à l'Energie Atomique, Saclay, France, kk2000@semt1.smts.cea.fr, available free for universities) and were run either on a SGI O_2 or a standard PC.

In engineering terms, strain (ε) is defined as a change in length (dl) per unit length (l): $\varepsilon = dl/l$. Strain has no unit and is given either in percent or in microstrain ($\mu\varepsilon$) with 10,000 $\mu\varepsilon = 1\%$. Tensile strains are represented by positive values of ε, and negative values of ε indicate compressions. Poisson's ratio is the ratio of transverse contraction strain to longitudinal extension strain in the direction of stretching force.

Microscopy observation of the aspiration showed that the aspiration process did not affect the cell far from the location of aspiration, and therefore we only modeled the cellular region within a 10 μm radius of the axis of the pipette. In this region, the cell and the pipette were assumed to be symmetrical around the axis of the pipette, and the cell was modeled in two dimensions representing only one quarter plane using axisymmetric coordinates. The cytoplasm was modeled as a quarter plane meshed with three-noded triangular elements with higher densities in areas where large deformations were expected. The cytoplasmic Poisson ratio was chosen to be $\nu_{cyt} = 0.3$ (Maniotis et al., 1997). The cytoplasmic elasticity $E_{cyt} = 75$ Pa was empirically chosen as the elasticity for which the simulations best fit the experimental data from Fig. 3 *D* and is comparable to values measured experimentally with micropipette aspiration (Theret et al., 1988). The cortex and plasma membrane were modeled as thin elastic shells (Fig. 4, *inset*). The cortex was uniformly tethered to the cytoplasm on the under side and to the cell membrane on the upper side. The plasma membrane had a thickness of 3 nm, a Poisson ratio of $\nu_{memb} = 0.49$ and an elasticity of $E_{memb} = 10$ kPa (calculated from the area expansion modulus, the shear modulus, and the thickness of the cell membrane given in Hamill and Martinac, 2001). The actin cortex had a thickness t of 0.1 μm (inferred from immunostaining and confocal microscopy examination, data not shown), a Poisson ratio ν_{cortex} of 0.3 and an elasticity $E_{cortex} = 300$ Pa (in line with values found for actin networks cross linked with α-actinin, Tseng and Wirtz, 2001). The cell was not allowed to move on the under side (*triangles* in Fig. 4) and was allowed to move in the z direction along the axis of symmetry (sliding contacts in Fig. 4). On the top side, the micropipette was represented by an L-shaped line with rounded edges (to facilitate computational sliding) resting on the top surface of the cell (in *red*, Fig. 4). A no-penetration contact boundary condition was imposed between the cell membrane and the pipette. Several groups have experimentally examined adhesion between the micropipette glass and the cell membrane (Opsahl and Webb, 1994; Sokabe et al., 1991). We modeled the adhesion between the glass and the membrane as a force exerted at the center of each membrane element in contact with the glass and at an angle θ with the membrane element (*inset*, Fig. 4). Reported orders of magnitude for the adhesion γ of cell membrane to glass range from 0.1 to 1 dynes.cm^{-1} (= 10^{-4}–10^{-3} N.m^{-1}, Opsahl and Webb, 1994) and the angle θ ranges from 45 to 75° (Opsahl and Webb, 1994; Sokabe et al., 1991). In our simulations, we chose $\theta = 75°$ and $\gamma = 10^{-4}$ N.m^{-1}, as simulations with these values best fit the data. A hydrostatic pressure was applied at the mouth of the pipette (represented by the letter *P* in Fig. 4).

To simulate the cellular deformation in response to large hydrostatic pressures, we adopted an iterative approach. Briefly, a small increment of pressure (40 Pa) was applied onto the undeformed cell. The resulting deformation was calculated using a step-by-step iterative approach, implemented in CAST3M that is necessitated because of the large displacements resulting from the aspiration. The deformed surface was then remeshed and another pressure increment applied. For each step, the mesh and displacement fields were stored. When the desired pressure was reached, it was possible to calculate the strain distribution resulting from the complete aspiration process.

Initially, the cell was modeled as a solid with linear elastic and isotropic material properties. To examine the effect of the mechanical parameters on the strain distribution and bleb ''height'', the pressure P, the pipette radius R, the pipette opening angle α, the cytoplasmic elasticity E_{cyt}, the cytoplasmic Poisson ratio ν_{cyt}, the cortical elasticity E_{cortex}, the cortical Poisson ratio ν_{cortex}, the cortical thickness t, and the glass-membrane adhesion γ were

varied in turn while keeping the other variables constant. The standard values were $P = 600$ Pa, $R = 1.5$ μm, $\alpha = 1\ 0°$, $E_{cyt} = 75$ Pa, $\nu_{cyt} = 0.3$, $E_{cortex} = 300$ Pa, $\nu_{cortex} = 0.3$, $t = 0.1$ μm, and $\gamma = 10^{-4}$ N.m^{-1}. The values of the elasticities of the cytoplasm and the cortex are in line with experimentally derived values for whole cells (Theret et al., 1988).

When the cell was assumed to be purely linear elastic, the simulated curve relating membrane projection into the pipette to applied pressure followed an exponential law for tapered pipettes (as shown in Appendix I and Fig. 6 *A*) and did not match the experimentally measured curve that resembled a power law. To better simulate the experimental curve, linear stiffening and thickening of the actin cortex in response to strain were incorporated into the model, as experimentally observed by several groups (Glogauer et al., 1998; Merkel et al., 2000; Sokabe et al., 1991). To simulate the experimental curve, the cortical elasticity E_{cortex} was linked to the maximal membrane radial strain $\varepsilon_{rr,max}$ (Appendix I, ''Bleb expansion with linear stiffening''):

$$E_{cortex}(\varepsilon_{rr,max}) = e_{cortex} + e_1\varepsilon_{rr,max}(1 - e^{-(\varepsilon_{rr,max}/\varepsilon_Y)^2}), \quad (1)$$

with e_{cortex} the original Young's modulus, e_1 the rate of linear stiffening of the cellular material with applied strain, $\varepsilon_{rr,max}$ the maximal cellular radial strain, and ε_Y a strain scaling factor. The rate of the cellular stiffening e_1 and the scaling strain ε_Y were determined empirically by choosing values for which the simulation best fitted the experimental curve of the membrane extension into the pipette as a function of pressure. A similar evolution was used to describe the change in cortical thickness as a function of strain:

$$t_{cortex}(\varepsilon_{rr,max}) = t_{cortex} + t_1\varepsilon_{rr,max}(1 - e^{-(\varepsilon_{rr,max}/\varepsilon_Y)^2}). \quad (2)$$

Curve fitting

All curve fitting was performed using a least-squares approach in KaleidaGraph.

The experimental curve, relating the bleb ''height'' h to the pressure applied P, and the FE model simulated curves were fitted with the following function (weighted by the number of measures in the case of the experimental curve) that was derived from the theoretical model detailed in Appendix I, ''Bleb expansion if no linear stiffening is present (tapered pipettes)'' and ''Bleb expansion with linear stiffening'':

$$h(P) = aPe^{bP}e^{-(P/c)^2} + dP^f(1 - e^{-(P/c)^2}), \quad (3)$$

where a, b, c, d, and f are the parameters to be fitted. The first part of the curve combines the initial bleb formation with the theoretical exponential increase of height with pressure at low values of P for tapered pipettes (when no strain stiffening is observed), described in Appendix I, ''Bleb expansion if no linear stiffening is present (tapered pipettes)''. The second part of the curve represents the experimentally observed power-law increase in height with pressure when strain stiffening has started to occur at high values of P, described in Appendix I, ''Bleb expansion with linear stiffening''. The exponential functions serve to combine both curves into a continuous function.

In all cases, we used the value of r^2 as a measure of the goodness of fit.

RESULTS

Electrophysiology

Mechanosensitive ion channel activity was detected in primary osteoblasts with suction pressure application (Figs. 1 *A* and 2 *A*). Indeed, at high suction pressure, channels were very active and several channels could open simultaneously (e.g., for the pressure $P = -12$ kPa in Figs. 1 *A* and 2 *A*). A total of 99 cells were examined and the presence of mechanosensitive channels was detected in 44 cells (44%). Cells cultured for 48 h or 72 h showed a similar sensitivity to mechanical strain, and the proportion of cells in which stretch-activated channels were detected was not significantly different (chi-square test, $p = 0.16$). There was no difference in the proportion of cells displaying mechanosensitive channels when the electrode contained K-Ringer (reference solution, $n = 44$), Na-Ringer ($n = 24$, $p = 0.53$), K-Asp ($n = 12$, $p = 0.16$), or 70 KCl-65 NaCl ($n = 14$, $p = 0.08$). In all cases, the reversal potential of the ion channels was close to 0 mV (Fig. 1 *B*). These data are indicative of the presence of a nonselective cation channel. For all conditions, this channel had a conductance of 15 pS (Fig. 1 *B*).

The average pressure of first opening was 8.9 ± 3.7 kPa and the lowest pressure of first opening was 2.7 kPa (Fig. 2 *B*). The channel open probability (P_{open}) was plotted as a function of applied pressure (obtained from nine experiments, Fig. 2 *C*) and, when fitted with a sigmoid curve, revealed that, on average, the channels were open 50% of the time at 14 kPa. Channel openings were detected within 1 s of pressure application, but closed before pressure was released (Fig. 2 *A*).

With gadolinium chloride in the pipette, no channel openings were detected (0 out of 13 cells examined). When gadolinium was omitted from the electrode solution on the same day, mechanosensitive channels were observed with an equal frequency to other osteoblast cultures tested (6 out of 11 cells examined), thereby excluding the possibility of a nonresponsive cell preparation. These data showed that gadolinium chloride significantly blocked suction elicited channel openings (chi-square test, $p < 0.001$). Taken together, these data are indicative of nonselective stretch-activated cation channels in primary osteoblasts.

Video microscopy

The membrane extension was seen in the micropipette upon suction (Fig. 3 *A*) and its ''height'' could be determined (shown on Fig. 3 *B*). An increment in suction pressure caused further extension of the membrane into the pipette (Fig. 3, *D* and *E*). When the pressure was released, the length of the membrane extension within the pipette diminished, but the aspirated membrane did not completely retract, as would be expected if the deformation had been entirely elastic (Fig. 3 *E*). Therefore, micropipette aspiration deforms the cell with a mixture of elastic and plastic deformations. By averaging the experimental results over 12 cells, a representative curve relating the membrane extension into the micropipette and the applied suction pressure was generated (Fig. 3 *D*). The curve rose rapidly from the origin, reaching a height of 18 μm for 1.2 kPa. The rate of change then decreased, rising from 18 μm for 1.2 kPa to 25 μm for 15 kPa. This was suggestive of the

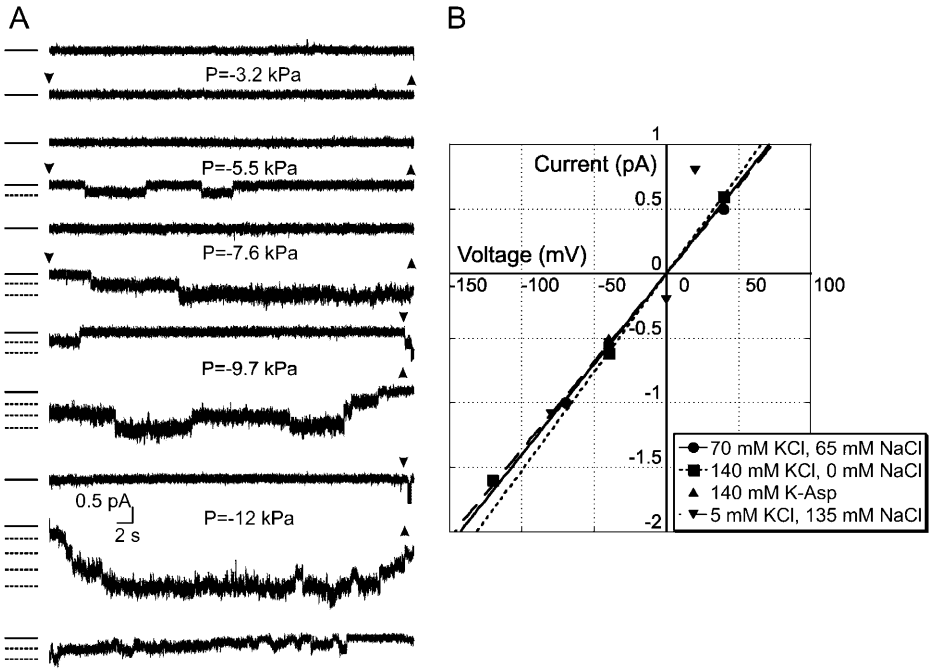

FIGURE 1 Pressure application through micropipette aspiration elicits opening of mechanosensitive channels in primary osteoblasts. (*A*) Single-channel currents in primary osteoblasts were activated by suction. Upon release of suction pressure, the channels returned to their closed state. The channels had small conductances (15 pS) and were very active during pressure application. A downward arrow indicates the beginning of pressure application and an upward arrow the release of pressure. No holding potential was applied. The applied suction pressure is given in kPa (1 mm Hg = 0.133 kPa). The zero current level is indicated by the solid line. Open channel current levels are indicated by dashed lines. (*B*) Current/voltage relationship for stretch-activated channels for different electrode solutions. Weighted linear functions were fitted to the data points except for the K-Asp solution, for which only one data point was available. In all cases, the reversal potential was close to 0 mV, indicative of a nonselective channel. Replacement of Cl^- by aspartate did not affect the channel conductance or reversal potential.

presence of strain stiffening within the cell. The representative experimental curve (Fig. 3 *D*) could be well fitted with the exponential function prolonged with a power law derived from Appendix I ($r^2 = 0.90$).

Finite element modeling

The FE model (Fig. 4) was used to examine the influence of mechanical parameters such as the pipette diameter, the pipette opening angle, and the cellular properties on the membrane radial strains (Fig. 5). When the cell was considered purely elastic, the simulated bleb height increased exponentially with pressure (Appendix I, ''Bleb expansion if no linear stiffening is present (tapered pipettes)'', Fig. 5 *A*, *dotted line* in Fig. 6 *A*). When strain-stiffening and cortex-thickening were included, the representative experimental curve of the membrane aspiration was well described by the model (Fig. 3 *D*, Fig. 5 *A*, *solid line* in Fig. 6 *A*). Thus, the model can accurately depict the experimental changes in membrane height observed during micropipette aspiration. Accordingly, the membrane strain and tension can be calculated with the model and related to the experimentally observed channel activity for any applied pressure. In this section, we will first describe the results of the FE simulations and then relate this to the biological experiments.

Strain distributions

In the simulations, the cell was only noticeably deformed in the vicinity of the aspirated material in agreement with experimental observations. The highest membrane tensile radial strains (ε_{rr}) were present on the surface of the bleb cap, whereas the highest compressive radial strains were present in the region of contact between the bleb and the pipette (Fig. 5 *A*). Tensile radial strains were also present at the pipette rim. The von Mises stresses were highest in the bleb at the contact between the pipette and the membrane near the pipette rim (Fig. 5 *B*). From experimental data by Wu et al. (1998) and Appendix II, plastic deformations would be expected in the cell for von Mises stresses superior to 75 Pa (the zone of expected plastic deformation is indicated in Fig. 5 *B*). Fig. 5, *A* and *B*, were computed for $P = 600$ Pa, $R = 1.5$ μm, $\alpha = 10°$, $E_{cyt} = 75$ Pa, $\nu_{cyt} = 0.3$, $E_{cortex} = 300$ Pa, $\nu_{cortex} = 0.3$, $t = 0.1$ μm, $E_{memb} = 10$ kPa, $\nu_{memb} = 0.49$, and $\gamma = 10^{-4}$ N.m^{-1}.

The graph of the membrane radial strains (ε_{rr}, Fig. 5 *C*) as a function of the distance s to the center of the pipette in the unstrained model (when pressure is applied, s can be interpreted as a curvilinear coordinate, shown in Fig. 5 *A*) presented three distinct zones. At the center of the pipette on the bleb apex, the cell membrane is submitted to tensile strains (Fig. 5, *A* and *C*, for abscissa $s = 0$ μm). In the zone of the bleb where the membrane and the pipette are in contact, the membrane is exposed to compressive strains (Fig. 5, *A* and *C*, for abscissa $s = 1$ μm). At the inner rim of the pipette, the cell membrane is under tension but membrane strain was ~2-fold lower than at the bleb cap (Fig. 5, *A* and *C*, for abscissa $s = 1.5$ μm). Finally, far from the pipette center, the strains converge toward zero, thereby justifying the assumption that, far away from the aspirated region, the cell is unaffected (Fig. 5 *C*). The membrane tension had similar distribution to the membrane

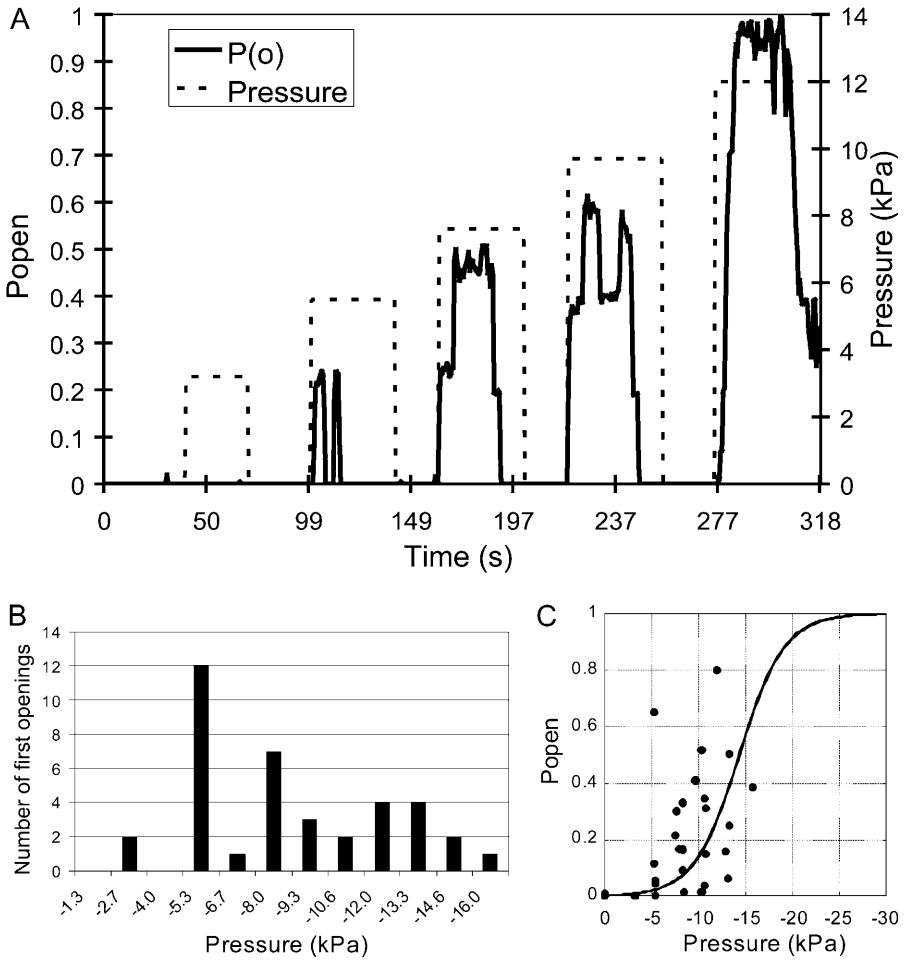

FIGURE 2 Evolution of channel open probability with time and pressure. (*A*) Open probability (P_{open}) and applied pressure as a function of time for the experiment shown in Fig. 1 *A* assuming that all of the channels present in the patch of membrane were observed. The phases of pressure application and their intensity are shown by the dotted line. The open probability is shown by the solid line. In all cases, channels opened within 1 s of pressure application, but closed before the release of pressure. This may be due to active adaptation processes triggered by mechanosensitive ion channel openings. The total number of channels open was a function of the magnitude of the pressure challenge. Up to five channels were active simultaneously in the patch of membrane. (*B*) Number of openings, which were first openings, as a function of pressure. A first opening was defined as the pressure for which the first stretch-activated current was detected. This graph was generated with data from 38 different experiments, each on a different cell. (*C*) Open probability (P_{open}) as a function of pressure applied. The open probability was calculated assuming that all of the channels in the patch had been observed during suction pressure application. The data points pertain to nine different experiments. The spread of the data arises from patch heterogeneity. A sigmoid curve was fitted to the data to yield an estimate of the pressure needed to open 50% of the channels.

strain with a maximum at the apex and a secondary maximum at the pipette rim (modeling data not shown).

Influence of mechanical parameters on linear elastic models

The influence of mechanical parameters was examined by plotting the membrane radial strains in the FE model (ε_{rr}) as a function of the distance s to the center of the pipette in the unstrained model. When the pressure is applied, s can be interpreted as a curvilinear coordinate (shown in Fig. 5 *A*). In all cases, the variables whose influences were not being examined were kept constant with the values given in the previous paragraph.

The opening angle α of the pipette, the pipette radius, and the cortical Poisson ratio had little or no influence ($<10\%$ variation) on the magnitude of the radial strains found in the cell membrane at the bleb apex (modeling result not shown). When membrane adhesion to the glass γ was increased, the membrane extension into the pipette decreased for a constant pressure. Membrane strains did not significantly decrease even though the membrane extension into the pipette did (modeling data not shown).

The cytoplasmic Poisson ratio ν_{cyt} had a drastic effect on the magnitude of strain elicited by aspiration (Fig. 5 *D*). The maximal radial strain varied from 4.8 for $\nu_{cyt} = 0.2$ to 0.4 for $\nu_{cyt} = 0.49$ (Fig. 5 *D*, for abscissa $s = 0$ μm). Increasing cytoplasmic Poisson ratio reduced the length of the membrane extension into the pipette for a given applied pressure (modeling results not shown).

The cytoplasmic elasticity E_{cyt} had a large effect on the magnitude of strains elicited. Increasing values of E_{cyt} reduced the magnitude of elicited radial strains (Fig. 5 *C*), as would be expected from the theoretical derivations of the expression of bleb height as a function of pressure and elasticity given in Eq. 9, Appendix I. Increasing cortical elasticity E_{cortex} and cortical thickness t reduced membrane extension into the pipette as well as membrane strains (Fig. 5, *E* and *F*).

Cellular strain needed to open mechanosensitive channels

The membrane extension into the micropipette as a function of suction pressure fitted the representative experimental data curve well when the FE model incorporated cell stiffening

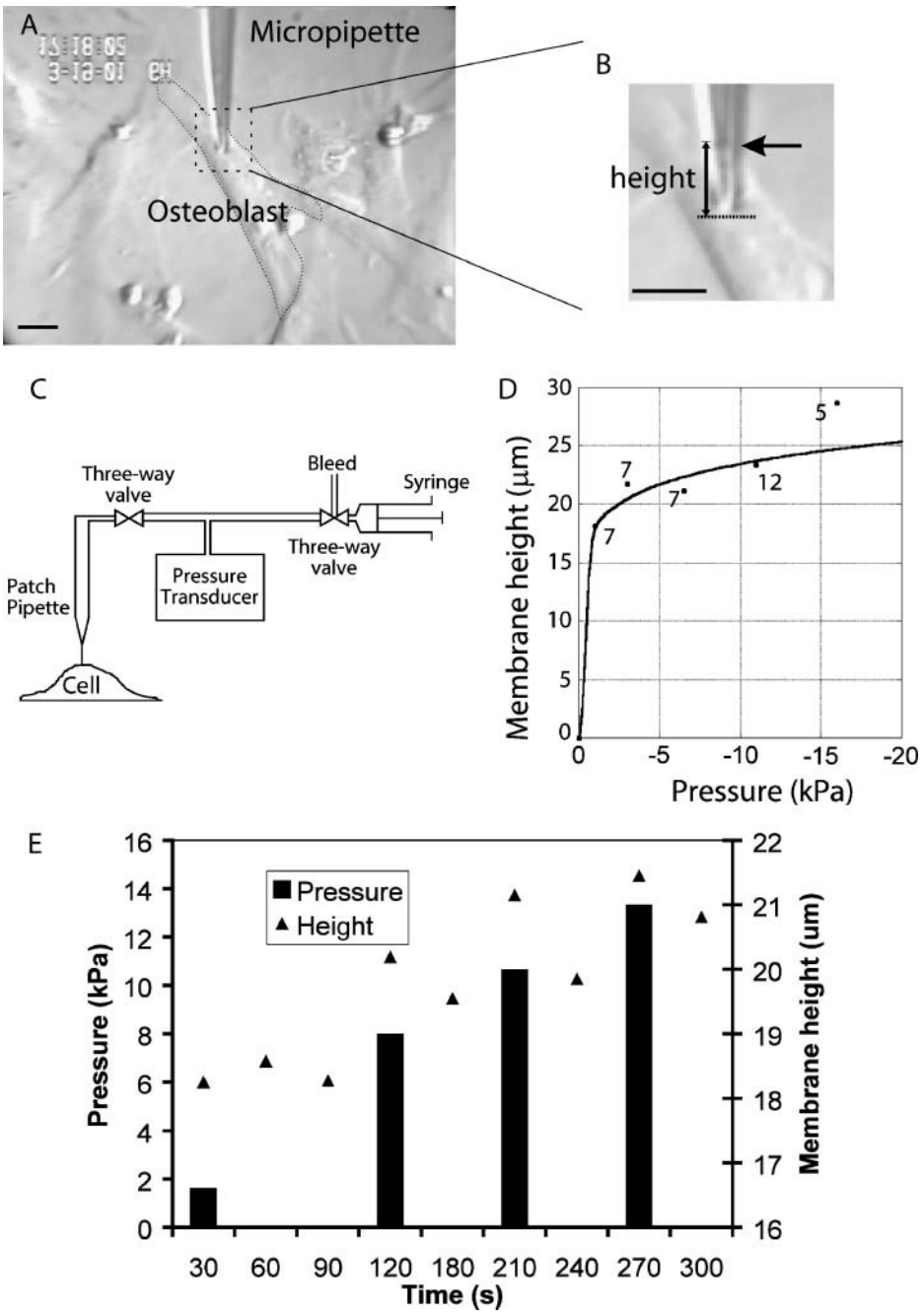

FIGURE 3 Video microscopy of membrane aspiration into the micropipette. (*A*) Hoffman optics image of a typical experiment. The bleb of membrane from the examined cell (an osteoblast, outlined with the *dotted line*) can be resolved in the micropipette. Bar, 10 μm. (*B*) Expanded region from boxed region in *A*, where the arrow indicates the tip of the bleb. The estimated height is indicated. Bar, 5 μm. (*C*) Diagram of the mechanical arrangement of the pressure application system. (*D*) Membrane height as a function of applied pressure. Each data point was averaged over several experiments and the number of experiments is indicated on the graph. The data were fitted with the weighted curve given in the Methods section. (*E*) Membrane height and applied pressure for different time points of a representative experiment. The bleb extension decreased when pressure was released but did not totally relax, showing the presence of plastic deformations.

(*solid curve*, Fig. 6 *A*). The experimental curve was best fitted when the FE simulation parameters were set to $e_{\text{cortex}} =$ 300 Pa, $e_1 = 50$ kPa, $\varepsilon_Y = 4.75$, $\nu = 0.3$, $R = 1.5$ μm, $\alpha = 10°$, $E_{\text{cyt}} = 75$ Pa, $\nu_{\text{cyt}} = 0.3$, $\nu_{\text{cortex}} = 0.3$, $t = 0.1$ μm, $E_{\text{memb}} = 10$ kPa, $\nu_{\text{memb}} = 0.49$, and $\gamma = 10^{-4}$ N.m^{-1}.

The curve that best fitted the experimental data could then be used to calculate the membrane strain magnitudes (Fig. 6 *B*) resulting from applied pressures corresponding to the experimentally derived levels needed to first open stretch-activated channels (Fig. 2 *B*) or for them to be active 50% of the time (Fig. 2 *C*). By combining the simulated curve relating membrane extension in the micropipette to applied pressure (Fig. 6 *A*) with the experimental data relating channel open probability to applied pressure (Fig. 2 *C*), we generated a curve relating the channel open probability to membrane strain and tension at the bleb apex (Fig. 6 *C*). The average pressure needed to obtain a first mechanosensitive channel opening was 8.9 kPa (Fig. 2 *B*). In the FE simulation, this corresponded to a membrane extension of 23 μm into the micropipette (Fig. 6 *A*), the maximal membrane radial strain predicted at the bleb apex was $\varepsilon_{\text{rr,max}} =$ 8.1 (Fig. 6 *B*), and the maximal membrane tension was 4.59

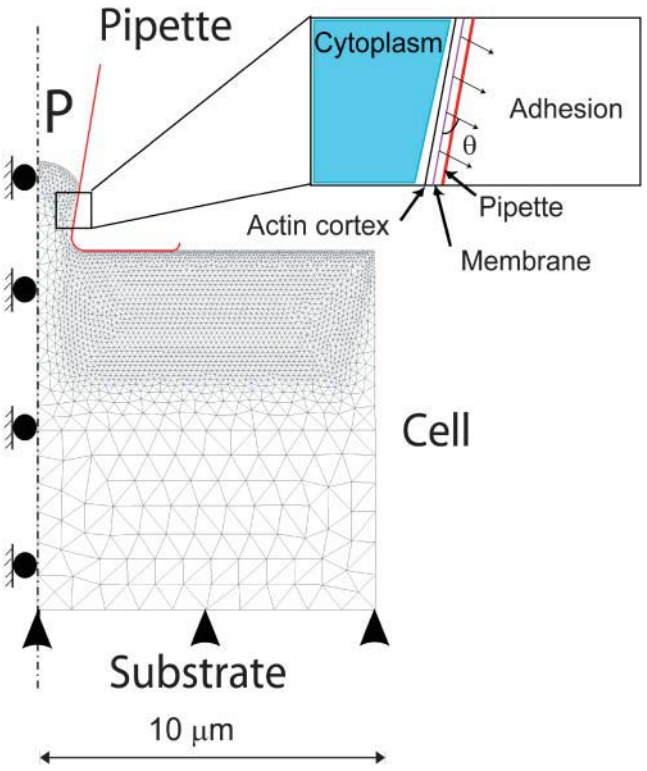

FIGURE 4 Finite element model of the pipette aspiration process. The cell was not allowed to move on the underside (*arrowheads*). The cell could freely slide along the axis of symmetry of the model. The pipette is shown in red. Pressure P was applied only in the area delimited by the pipette. The mesh was finer in areas where large deformations were expected to occur, such as on the cell surface. The top surface of the model incorporated a membrane and an actin cortex which were modeled as thin shells (*inset*). In the regions where the cell and the pipette interacted, an adhesion force (*arrows*, *inset*) was applied onto the cell membrane at an angle θ.

10^{-4} N.m^{-1}. The experimental electrophysiological data revealed that the pressure needed for the channels present in the patch of membrane to be open 50% of the time was 14 kPa (Fig. 2 *C*). In the FE simulation, the membrane extension into the micropipette reached a height of 25 μm for this pressure, the predicted maximal cellular radial strains on the bleb cap reached $\varepsilon_{rr,max} = 8.2$, and the predicted maximal membrane tension was 5 10^{-4} N.m^{-1} (Fig. 6 *C*).

Variation of cortical properties with applied strain

Once the membrane strain reached a certain threshold, the cortical elasticity varied linearly with the maximal membrane strain ($\varepsilon_{rr,max}$) and attained a value of 39 kPa for $\varepsilon_{rr,max} = 8.1$ (Fig. 6 *D*). The thickness of the actin cortex was 2.7 μm for such a strain and varied similarly with $\varepsilon_{rr,max}$. Both of these values are consistent with values observed in cells (Lehenkari et al., 1999).

DISCUSSION

In this study, we use a combination of experimental and computational modeling techniques to gain new insights into cell mechanics and the regulation of stretch-activated channels. We estimate the membrane strain and tension needed to elicit mechanosensitive channel openings in living cells. We demonstrate that primary osteoblasts possess nonselective stretch-activated cation channels and report the average suction pressures needed to elicit their opening and maintain them open 50% of the time. Experimentally measured membrane extensions into the micropipette in response to aspiration were averaged to create a ''representative experiment'' that was simulated using a finite element model incorporating the cell cytoplasm, actin cortex, and membrane. Stiffening of the cellular actin cortex with applied strain needed to be included into the model to simulate the experimental curve relating bleb extension into the pipette to applied pressure. From the simulated aspiration process, we found that maximal membrane strains of 8.2 and tensions of 5 10^{-4} N.m^{-1} were needed to maintain the channels open 50% of the time (Fig. 6 *C*). We examined the effect of relevant mechanical parameters on membrane strains. These data will help our understanding of the cellular mechanisms of strain detection through mechanosensitive channel opening.

Presence of stretch-activated channels in primary osteoblasts

Cells of the osteoblastic lineage play a fundamental role in the detection and adaptation of bone to mechanical stimuli; however, questions remain about the mechanisms through which they detect mechanical stimuli. Mechanosensitive channels have previously been reported in permanent osteoblastic cell lines but not in primary cells, which better reflect the in vivo characteristics of this cell type. We have shown the presence of a pressure-sensitive nonselective cation channel with a 15 pS conductance in primary osteoblasts (Fig. 1 *B*). Using similar techniques, Davidson et al. (1990) showed the presence of two nonselective cation channel types with conductances of 20 and 50 pS in UMR-106 osteosarcoma cells. Duncan and Misler (1989) reported the presence of an 18 pS stretch-activated channel in osteoblastic G292 cells. In primary cells, the channels opened in response to pressure and were active during the pressure application period, closing shortly before the pressure was released (Fig. 1 *A* for $P = -12$ kPa, Fig. 2 *A*). Some channels had bursts of openings lasting well over a second (such as in Fig. 1 *A*). Although uncommon, such long openings have also been observed in CHO cells transfected with the yeast stretch-activated cation channel MID1 (Kanzaki et al., 1999). The average pressure at which the first channel openings were observed was 8.9 kPa (67 mm Hg, Fig. 2 *B*) and the average pressure needed for the

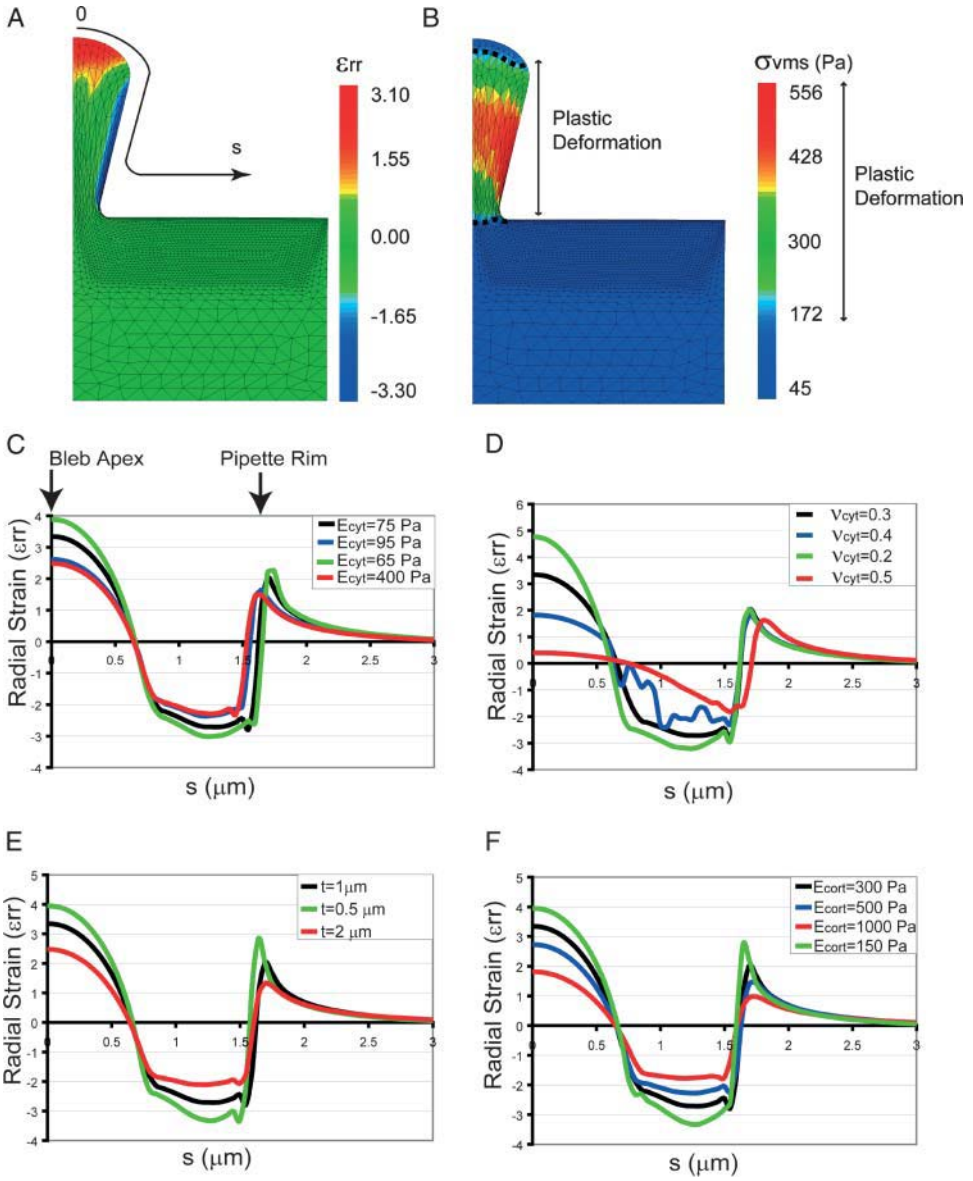

FIGURE 5 Results of the finite element simulations for a linear elastic material with no linear stiffening. (*A*) Radial strain (ε_{rr}) distribution due to micropipette aspiration. Large tensile radial strains (shown in *red*) occur at the tip of the bleb and at the inner rim of the pipette. Compressive radial strains (shown in *blue*) are elicited in the regions where the bleb and the pipette are in contact. (*B*) Von Mises stress distribution due to micropipette aspiration. Large von Mises stresses occur at the bleb surface in the vicinity of the inner rim of the pipette. Using the results from Appendix II, the zone where plastic deformations occur is indicated with dotted lines. In *C*, *D*, *E*, and *F*, the radial strain is plotted as a function of *s*, the distance to the center of the pipette in the undeformed model. In the deformed model, *s* can be interpreted as a curvilinear coordinate (shown in *A*). (*C*) Radial strain (ε_{rr}) at the surface of the cell as a function of distance (*s*) to the pipette central axis for different cytoplasmic elasticities (E_{cyt}). (*D*) Radial strain (ε_{rr}) at the surface of the cell as a function of distance (*s*) to the pipette central axis for different cytoplasmic Poisson ratios (ν). E. Radial strain (ε_{rr}) at the surface of the cell as a function of distance (*s*) to the pipette central axis for different cortical thicknesses (*t*). (*F*) Radial strain (ε_{rr}) at the surface of the cell as a function of distance (*s*) to the pipette central axis for different cortical elasticities (E_{cort}).

channels to be open 50% of the time was ~14 kPa (105 mm Hg, Fig. 2 *C*). These pressures were similar to those required in neurons or smooth muscle cells (Wan et al., 1999; Zou et al., 2002). Mechanosensitive channels could be the first step in the transduction of external mechanical stimuli into whole cell responses. In support of this, two groups (Kirber et al., 2000; Zou et al., 2002) have shown that mechanosensitive channel openings elicited by micropipette aspiration could give rise to whole cell cytosolic calcium reactions in smooth muscle cells even when calcium was omitted from the electrode solution. Mechanosensitive channels outside of the pipette are unlikely to open because the strain and tension are twofold lower than in the pipette. Therefore, the entry of cations through the stretch-activated channels suffices to depolarize the cell and trigger the entry of Ca^{2+} into the whole cell via voltage-activated Ca^{2+} channels (Kirber et al., 2000). From a physiological standpoint, the small conductance of the stretch-activated channels observed in bone cells may modulate cell sensitivity to mechanical strain in two different ways. Channels with a small conductance will only depolarize the cell sufficiently to elicit a whole cell calcium transient if the stimulation is very prolonged or if it opens a large proportion of the cellular stretch activated channels. In contrast, brief localized stimulations may not give rise to large enough depolarizations to elicit whole cell calcium transients. As bone adaptation is a costly process both in time (~6 weeks) and in energy, unnecessary adaptations need to be avoided and having mechanosensitive channels with a small conductance may help to select for only prolonged stimulations or those applied to whole cells.

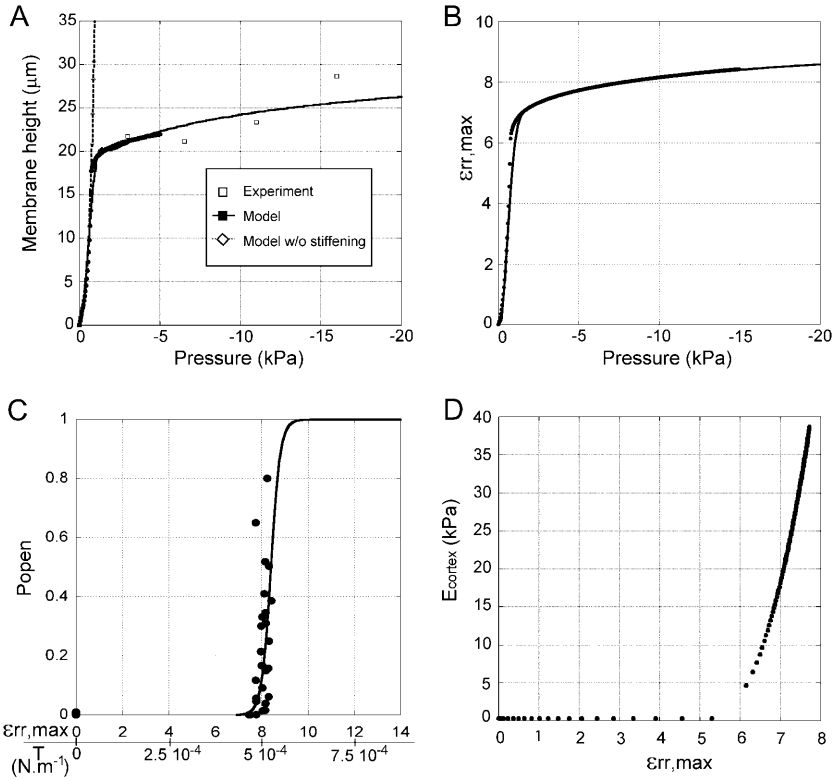

FIGURE 6 Results of the finite element simulations for the models incorporating linear stiffening. (*A*) Experimental (□) and simulated (■) lengths of membrane extension into the micropipette as a function of the applied suction pressure. The data were fitted with Eq. 3. The simulated curve incorporating linear stiffening (*solid line*) closely follows the experimental data points for the parameter values $E_{cyt} = 75$ Pa, $E_{cort} = 300$ Pa, $e_1 = 50$ kPa, and $\varepsilon_Y = 0.01$. When the simulation did not incorporate linear stiffening, the simulated membrane extensions diverged (*dotted line*). (*B*) Maximal radial strain ($\varepsilon_{rr,max}$) as a function of applied pressure for the set of parameters that best fit the experimental data (*dotted line* in *A*). The simulated data points were fitted with the same type of curve as in *A*. (*C*) Open probability (P_{open}) as a function of membrane strain ($\varepsilon_{rr,max}$) and membrane tension (T). The open probabilities were derived experimentally from Fig. 2 *C* and plotted as a function of the calculated maximal radial strain ($\varepsilon_{rr,max}$, shown in *B*) and maximal membrane tension (T) resulting from the experimental pressure at which they were collected. The spread of the data observed in Fig. 5 *F* has been drastically reduced due to the saturation of membrane extension with pressure (Fig. 3 *D*). A sigmoid curve was fitted to the data to yield an estimate of the strain and tension needed to open 50% of the channels. (*D*) Curve showing the evolution of the cortical elasticity as a function of the maximal membrane strain elicited by the applied suction pressure (*curve* shown in *B*).

Strain magnitude needed to elicit stretch-activated channel opening

Finite element modeling enabled us to simulate bleb aspiration into the pipette and calculate the strain distributions in the aspirated bleb of membrane. Membrane radial tensile strains and membrane tension (discussed in the next paragraph) are the most likely mechanical parameters to be detected by mechanosensitive channels as they physically stretch the cellular material and are maximal on the surface of the bleb apex. The predicted membrane radial tensile strains needed to open stretch-activated cation channels in osteoblasts (800%) were more than two orders of magnitude larger than those needed to elicit whole cell increases in cytosolic calcium concentration in response to AFM microindentation (2.5%), which can also be mediated by mechanosensitive channels (Charras and Horton, 2002). Furthermore, this strain magnitude by far exceeds the lytic strains for an unsupported lipid bilayer (3–5%; Sachs and Morris, 1998). Several factors may explain how such a large strain magnitude can be applied onto the cells.

First, the structure of the cell membrane and subplasmalemmal cytoskeleton is complex and poorly understood. The subplasmalemmal cytoskeleton is a complex structure made up of a fine mesh of spectrin, actin, and other proteins, which regulates cytoskeletal attachment to the cell membrane and membrane infolding. Indeed, the cell membrane possesses excess area that may reach 100 to 1000% (Hamill and Martinac, 2001), present in the form of folds or villi or in the cell cytoplasm in the form of vacuoles (Dai et al., 1998; Raucher and Sheetz, 1999; McNeil et al., 2000; Mills and Morris, 1998). These details were not included in our model of the cell membrane and actin cortex as none are well enough characterized quantitatively. Hence, during a large part of the aspiration process, the cell can accommodate the increase in membrane area caused by the extension of the bleb by unfolding membrane invaginations or by adding membrane stored in the cytoplasm in the form of vesicles (McNeil et al., 2000; Mills and Morris, 1998). In our study, the volume of the aspirated bleb at mechanosensitive channel opening (calculated from Eq. 4, Appendix I, ''Bleb expansion if no linear stiffening is present (tapered pipettes'', and the representative experiment, $V_b = 352\ \mu m^3$) is small compared to the total volume of a cultured cell ($V_c = 4200\ \mu m^3$ on average; Charras and Horton, 2002). Consequently, the extra membrane needed to accommodate this change in volume of $<10\%$ could easily be recruited.

Second, the aspiration process likely mechanically disrupts the cytoskeleton, whereas AFM microindentation is minimally damaging to the actin or microtubule cytoskeleton (Charras and Horton, 2002). Large von Mises stresses are present within the bleb and these reach a level where plastic deformations are expected to occur (Appendix II). Plastic deformations, corresponding to the disruption of the cytoskeleton at the base of the bleb, would help dissipate some of the applied strain.

Third, our experimental results revealed that the cell adapted its elasticity to applied strain. Such processes have

been observed in living cells by other groups. These have been hypothesized to arise from either passive processes due to the linear stiffening properties of the cellular cytoskeleton at large strains (Ingber, 1993; Wang et al., 2001) or from active cytoprotective processes (Choquet et al., 1997; Glogauer et al., 1998). Indeed, cells submitted to prolonged pulling by a magnetic microbead form actin patches under the area of stimulation (Glogauer et al., 1998). Similarly, cells challenged by microbead pulling strengthen their cytoskeleton/integrin linkage to better resist pull (Choquet et al., 1997). In the case of bleb aspiration, it is likely that, during the initial patch formation or the first pressure challenge, the cytoskeleton is disrupted at the mouth of the pipette (see the area of high von Mises stress in Fig. 5 *B*, in agreement with experimental data in *Dictyostelium* by Merkel et al., 2000) and attempts to reform in the aspirated bleb by targeting large quantities of F-actin and myosin II to that area (Merkel et al., 2000). Experiments examining phagocytosis of a yeast cell by a granulocyte revealed that forces are generated on the phagocytosed cell within 30 s of its engulfment into the cell (Evans et al., 1993). In our experiments, the closure of channels before pressure release and the cortical stiffening were observed within a similar time frame and therefore may be due to an active adaptational process (Figs. 2 *A* and 3 *D*). Similar adaptations of mechanosensitive channels in response to applied pressure have been observed by other groups (Hamill and McBride, 1992; Wan et al., 1999). The cortical stiffening may involve actin and myosin contraction to bring membrane tension below the threshold for mechanosensitive channel opening and attempt to restore the integrity of the actinous cortex. The values predicted in our simulation for the cortical elasticity (39 kPa) after adaptation remain well within the physiological range (Fig. 6 *D*) (Lehenkari et al., 1999), and the final thickness of the actin cortex (2.7 μm) is compatible with values reported by Merkel et al. (2000) (1.5–2 μm).

Membrane tensions needed to open stretch-activated channels

FE modeling results indicated that membrane tensions of 5 10^{-4} N.m^{-1} were needed to maintain stretch-activated channels open 50% of the time and that the gating curve for channel opening in response to membrane strain or tension was very steep (Fig. 6 *C*). Resting tensions in the cell membrane are estimated to be between 2.5 10^{-5} N.m^{-1} in leukemia cells (Dai et al., 1997) and 3 10^{-4} N.m^{-1} in fibroblasts (Thoumine et al., 1999). Hence, total membrane tensions on the order of 5–8 10^{-4} N.m^{-1} are necessary to open mechanosensitive channels in osteoblasts. This membrane tension is more than one order of magnitude lower than the membrane tensions reported to open the bacterial large conductance mechanosensitive channel MsCL (12 dynes.cm^{-1} = 1.2 10^{-2} N.m^{-1}, Sukharev et al., 1999) or yeast plasma membrane mechanosensitive channels (5 10^{-3} N.m^{-1},Gustin et al., 1988). These differences may stem from evolutionary differences in channel properties due to the different physiological stresses encountered by animal cells, yeast cells, and bacteria in their normal environment, and from the known differences in the structure of prokaryotic and eukaryotic cell membranes and walls.

If mechanosensitive channels sense membrane tension rather than membrane strains, the results of our previous AFM experiments (Charras and Horton, 2002) and the micropipette aspiration experiments in this study can be reconciled. Indeed, AFM stimulation acts on membranes with an intact submembranous cytoskeleton in contrast to experiments relying on aspiration into micropipettes where the submembranous cytoskeleton and its connections to the actin cortex are damaged (Merkel et al., 2000); hence the apparent stiffness of the membrane-cortex system in AFM experiments would be greater than that in micropipette aspiration experiments. Therefore the lower strain applied onto cells with an intact plasma membrane-actin cortex in AFM stimulation could translate into tensions similar to those generated by far higher strain on the more compliant membrane of aspirated cells.

Influences of mechanical parameters on the strain distributions elicited by micropipette aspiration

Modeling the bleb aspiration process into the micropipette enabled us to estimate membrane strain distributions within the bleb. The calculated membrane strains (Fig. 5) were in good agreement with experimentally observed and predicted strains in aspirated blebs from red blood cells (Lee et al., 1999). The cytoplasmic Poisson ratio, cytoplasmic elasticity, cortical elasticity, and cortical thickness greatly influenced the strain distributions elicited by micropipette aspiration (Fig. 5, *E* and *F*). Conversely, we demonstrate here that the radius of the pipette, the opening angle of the pipette, and the cortical Poisson ratio had little effect on the tensile radial strain distribution elicited at the bleb apex. These results underline potential strategies that the cell can use to react to a mechanical disruption. Indeed, the rapid assembly of a thick actinous cortex coupled with myosin II-mediated contraction observed within 30 s by Merkel et al. (2000) and Evans et al. (1993) is an efficient strategy to prevent further deformation and reduce membrane tension to below the threshold for stretch-activated channel opening. This may also explain why channels closed before the end of each pressure episode (Fig. 2 *A*).

Limitations

Certain issues still remain, beyond the limitations already discussed. First, for simplicity, the cell was modeled as a linear elastic material rather than a viscoelastic or viscoplastic material (Thoumine et al., 1999), and the cell was assumed to be a homogenous continuum rather than

a structure formed by discrete cytoskeletal elements. These are clearly oversimplifications. However, strain is a measure of local deformation between an initial state and a final state and is independent of the path followed to reach the final state. Hence, our model, though relating to a homogenous material, gives the correct macroscopic continuum strains. The exclusion of viscous properties does not affect the results of our study because only stationary solutions are sought. Second, to simplify modeling of the large deformations, we assumed that the superposition principle could be applied throughout the simulation. Third, we have not modeled the adhesion between the cell membrane and the actin cortex and hence cannot predict separation of the cell membrane from the cortex as observed by Oghalai et al. (1998). To date, the mechanisms of strain transmission between the cytoskeleton and the lipid bilayer are unknown (Ko and McCulloch, 2000). Fourth, we have assumed that the elasticity of the whole cell cortex changed in response to mechanical strain rather than just in the highly strained areas. This, although simplifying the modeling, may lead to an underestimation of the final elasticity.

CONCLUSION

In summary, we have combined single-channel recordings with mechanical modeling to enable us to simulate the process of micropipette aspiration and provide an estimate of the radial tensile strain needed to open stretch-activated channels in primary osteoblasts. We show that strains in excess of 800% were needed to open stretch-activated channels. This strain magnitude was much larger than the levels needed to elicit whole cell increases in cytosolic calcium concentrations through mechanosensitive openings by AFM microindentation. However, this could be explained if mechanosensitive channels were sensitive to membrane tension rather than strain. Our study underlines the need to gain a better understanding of the subplasmalemmal cytoskeleton and of the stress transmission between the cell cytoskeleton and the cell membrane.

APPENDIX I: THEORETICAL MODEL

The equations relating the initial creation of a spherical bleb of membrane within the pipette have been solved by Theret et al. (1988). However, we wanted to link the bleb ''height'' to the pressure applied for further stages of micropipette aspiration.

In all our derivations, we assumed that the cellular material was linear elastic and isotropic.

Bleb expansion if no linear stiffening is present (tapered pipettes)

We hypothesized that the micropipette had the shape of a cut cone with an opening angle 2 α (Fig. 7). The mouth of the pipette was at the height h_1 from the cone apex. The bleb of membrane was composed of two parts, one cut cone going from the mouth of the pipette at height h_1 to the height where

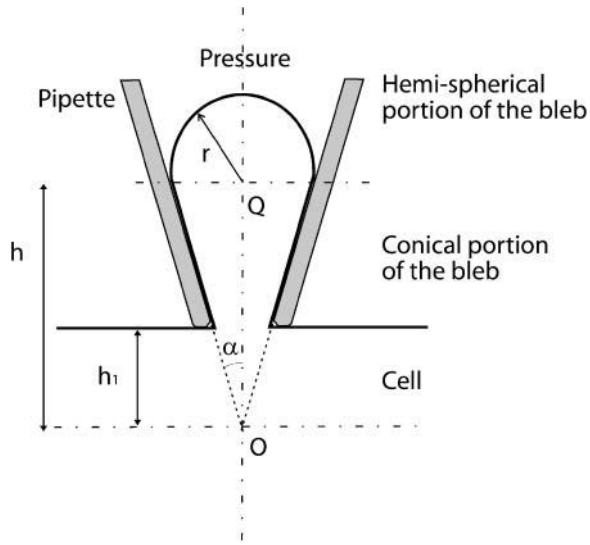

FIGURE 7 Diagram of the aspiration of a bleb of membrane into a micropipette. The micropipette was modeled as a cut cone. The cone apex is at O, h_1 is the height at which the pipette starts, h is the height at which the bleb of membrane separates from the pipette inner edge, and 2 α is the cone opening angle. The bleb of membrane was modeled as being composed of a conical and a hemispherical region. The conical region extended between height h_1 and h. The hemispherical region was centered in Q and had a radius $r = h.\tan(\alpha)$. The hydrostatic pressure was applied onto the hemispherical region.

the bleb separated from the pipette wall at height h, and one hemispherical part with radius $r = h.\tan(\alpha)$ (Fig. 7, in agreement with Sakmann and Neher, 1995). To simplify theoretical derivations, we assume that the shape of the bleb apex does not deviate from a hemisphere. The total volume of the bleb is

$$V_{\text{bleb}} = V_{\text{cone}} + V_{\text{hemisphere}} = \frac{\pi \tan^2(\alpha)}{3}(h^3 - h_1^3) + \frac{2}{3}\pi \tan^3(\alpha)\, h^3. \quad (4)$$

Hence, for a small variation of height dh, the variation in volume dV is

$$dV_{\text{bleb}} = \pi(2\tan^3(\alpha) + \tan^2(\alpha))\, h^2\, dh. \quad (5)$$

The hemispherical part of the bleb is the only part exposed to hydrostatic pressure and hence the problem is equivalent to that of a hemisphere exposed to hydrostatic pressure. Any radial displacement u_r caused by a small increment in pressure dP will translate into an increase in bleb height dh. The expression of u_r as a function of the pressure increment dP is (Timoshenko and Goodier, 1970)

$$u_r = \frac{(1-2\nu)}{E} r\, dP, \quad (6)$$

with ν the cellular Poisson ratio, E the Young's modulus, and r the radius of the sphere. Therefore, the variation in volume of the hemisphere, excluding second-order terms, is

$$dV = 2\pi r^2 u_r = 2\pi \frac{(1-2\nu)}{E} r^3\, dP. \quad (7)$$

Assuming that the volume variation of the hemispherical part of bleb is the main factor driving bleb ascension into the micropipette, we can write, knowing that $r = h\tan(\alpha)$,

$$\begin{aligned} dV = dV_{\text{bleb}} &\Leftrightarrow 2\pi\tan^3(\alpha)h^3\frac{(1-2\nu)}{E}dP \\ &= \pi(2\tan^3(\alpha)+\tan^2(\alpha))\,h^2\,dh \\ &\Leftrightarrow \frac{2\tan(\alpha)\,(1-2\nu)}{E(1+2\tan(\alpha))}dP = \frac{dh}{h}. \end{aligned} \tag{8}$$

By integrating the expression, we find

$$\begin{aligned} h(P) &= e^{(\psi(\alpha,\nu)\,\mathrm{p/E+c})} \\ \psi(\alpha,\nu) &= \frac{2\tan(\alpha)\,(1-2\nu)}{(1+2\tan(\alpha))} \end{aligned} \tag{9}$$

with c an integration constant that can be determined with the data from Theret et al. (1988). Indeed, the pressure P needed to create a hemispherical bleb cap (with the radius $r = h_1\tan(\alpha)$) within the micropipette is (Theret et al., 1988)

$$P = \frac{2\pi E}{3\Phi(\eta)} \tag{10}$$

$$\eta = \frac{b-a}{a}, \tag{11}$$

with E the Young's modulus of the cell, Φ the wall function of the pipette, η the wall parameter, b the outer diameter of the pipette, and a the inner diameter.

Bleb expansion if no linear stiffening is present (cylindrical pipettes)

Aspiration of a homogeneous half space or a layered material into cylindrical pipettes has been treated in detail respectively by Theret et al. (1988) and Alexopoulos et al. (2001). Briefly, if we consider the bleb to be composed of a cylinder and a hemisphere, and use the assumptions made previously, we get

$$V_{\text{bleb}} = V_{\text{cylinder}} + V_{\text{hemisphere}} = \pi r^2(h-h_1) + \frac{2}{3}\pi r^3, \tag{12}$$

and therefore

$$dV_{\text{bleb}} = \pi r^2 dh. \tag{13}$$

By equating with Eq. 7, we get

$$2\frac{(1-2\nu)}{E}r\,dP = dh. \tag{14}$$

Integrating Eq. 14, we get

$$h(P) = 2\frac{(1-2\nu)}{E}r\,\Delta P. \tag{15}$$

Therefore, with our simplified model, we get a linear relationship between the extension of membrane into the pipette and the suction pressure (in agreement with previous studies Alexopoulos et al., 2001; Theret et al., 1988).

Bleb expansion with linear stiffening

The experimental data curve relating bleb ''height'' to applied pressure resembles a power law at pressures >2 kPa. This implies that the material properties of the cell are a function of the applied pressure P and consequently of the applied strain ε: $E = f(P) = g(\varepsilon)$. The function relating h to P is of the form

$$h(P) = bP^{\mathrm{a}} = e^{\mathrm{a}\,\ln(\mathrm{P})+\ln(\mathrm{b})}. \tag{16}$$

If we take the natural logarithm of this expression and differentiate it, we get

$$\frac{dh}{h} = a\frac{dP}{P}, \tag{17}$$

and similarly, from Eq. 8, we get

$$\frac{dh}{h} = \psi(\alpha,\nu)\frac{dP}{E(P)}. \tag{18}$$

By equating Eqs. 12 and 13, we can write

$$E(P) = \frac{\psi(\alpha,\nu)}{a}P, \tag{19}$$

and hence E is a linear function of P.

APPENDIX II: ESTIMATING CELLULAR PLASTICITY

To infer the plasticity limit of osteoblasts, we decided to model the experiments performed by Wu et al. (1998) on fibroblasts using finite element modeling and elasticity measurements derived from micropipette aspiration measurements. Indeed, many different cell types have elasticities that fall into the same range when measured by AFM (Lehenkari et al., 2000; Radmacher, 1997) or by micropipette aspiration (Evans et al., 1976; Theret et al., 1988). Hence, we assumed that different cell types had similar ranges of plasticity limit. Wu et al. (1998) applied an indentation force of 10 nN onto a fibroblast using an AFM tip. After allowing a minute for recuperation, the resulting plastic deformations were measured. On average a plastic deformation of 0.43 μm was reported. The indentation depth can be calculated, knowing the reported elasticity E (2.24 kPa) and the applied force F (10 nN), using the formula giving the depth of indentation δ of a homogenous half plane by a cone (Johnson, 1985):

$$\delta = \sqrt{\frac{2F(1-\nu^2)}{E\pi\tan(\alpha)}} = 1.8\ \mu m, \tag{20}$$

with a Poisson ratio $\nu = 0.3$, and the half opening of the cone $\alpha = 60°$.

The cell was modeled as a quarter plane of 5 μm × 5 μm × 5 μm and was meshed with cubic elements with 20 nodes. The indentation was modeled using a step-by-step technique as described (Charras et al., 2001), except that the shape of the punch was pyramidal with an opening angle of 60°. The indentation depth applied was that calculated from the experiments of Wu et al. (1998). The elasticity of the material was chosen to be that inferred from the micropipette aspiration experiments (E = 75 Pa) and the Poisson ratio was chosen to be 0.3.

The plasticity limit was inferred from the levels of von Mises stresses at a depth equal to the permanent deformations experimentally noted. The resulting plasticity limit in these cells was 75 Pa.

The authors thank Jeff Dixon (University of Western Ontario, London, Ontario, Canada) for his insights and comments on the manuscript. G.T.C. thanks Thierry Charras (Commissariat à l'Energie Atomique, France) for his help and advice regarding the finite element modeling. Finally, the authors thank the reviewers for their constructive criticism of the text.

G.T.C. was in receipt of a Bogue International Fellowship from University College London. G.T.C. is most grateful to all of the members of the Dixon and Sims labs for their warm welcome and help during his stay in London,

Ontario. M.A.H. was supported by a Johnson & Johnson ''Focused Giving'' award, and by a program grant from The Wellcome Trust. S.M.S. and B.A.W. were supported by the Canadian Institutes of Health Research with grant No. MT10019, Heart and Stroke Foundation of Ontario with grant No. NA4944, and the Group in Skeletal Development and Remodeling.

REFERENCES

Alexopoulos, L., M. Haider, and F. Guilak. 2001. An axisymmetric elastic layered half-space model for micropipette aspiration of the chondrocyte pericellular matrix. *In* Advances in Biomedical Engineering. American Society of Mechanical Engineers, Snowbird, UT. BED-Vol. 51.

Chang, G., R. H. Spencer, A. T. Lee, M. T. Barclay, and D. C. Rees. 1998. Structure of the MscL homolog from *Mycobacterium* tuberculosis: a gated mechanosensitive ion channel. *Science.* 282:2220–2226.

Charras, G. T., and M. A. Horton. 2002. Single cell mechanotransduction and its modulation analyzed by atomic force microscope indentation. *Biophys. J.* 82:2970–2981.

Charras, G. T., P. P. Lehenkari, and M. A. Horton. 2001. Atomic force microscopy can be used to mechanically stimulate osteoblasts and evaluate cellular strain distributions. *Ultramicroscopy.* 86:85–95.

Choquet, D., D. P. Felsenfeld, and M. P. Sheetz. 1997. Extracellular matrix rigidity causes strengthening of integrin-cytoskeleton linkages. *Cell.* 88:39–48.

Dai, J., M. P. Sheetz, X. Wan, and C. E. Morris. 1998. Membrane tension in swelling and shrinking molluscan neurons. *J. Neurosci.* 18:6681–6692.

Dai, J., H. P. Ting-Beall, and M. P. Sheetz. 1997. The secretion-coupled endocytosis correlates with membrane tension changes in RBL 2H3 cells. *J. Gen. Physiol.* 110:1–10.

Davidson, R. M., D. W. Tatakis, and A. L. Auerbach. 1990. Multiple forms of mechanosensitive ion channels in osteoblast-like cells. *Pflugers Arch.* 416:646–651.

Discher, D. E., D. H. Boal, and S. K. Boey. 1998. Simulations of the erythrocyte cytoskeleton at large deformation. II. Micropipette aspiration. *Biophys. J.* 75:1584–1597.

Dixon, S. J., J. E. Aubin, and J. Dainty. 1984. Electrophysiology of a clonal osteoblast-like cell line: evidence for the existence of a Ca2+-activated K+ conductance. *J. Membr. Biol.* 80:49–58.

Drury, J. L., and M. Dembo. 1999. Hydrodynamics of micropipette aspiration. *Biophys. J.* 76:110–128.

Duncan, R., and S. Misler. 1989. Voltage-activated and stretch-activated Ba2+ conducting channels in an osteoblast-like cell line (UMR 106). *FEBS Lett.* 251:17–21.

Evans, E., A. Leung, and D. Zhelev. 1993. Synchrony of cell spreading and contraction force as phagocytes engulf large pathogens. *J. Cell Biol.* 122:1295–1300.

Evans, E. A., R. Waugh, and L. Melnik. 1976. Elastic area compressibility modulus of red cell membrane. *Biophys. J.* 16:585–595.

Glogauer, M., P. Arora, D. Chou, P. A. Janmey, G. P. Downey, and C. A. McCulloch. 1998. The role of actin-binding protein 280 in integrin-dependent mechanoprotection. *J. Biol. Chem.* 273:1689–1698.

Guharay, F., and F. Sachs. 1984. Stretch-activated single ion channel currents in tissue-cultured embryonic chick skeletal muscle. *J. Physiol.* 352:685–701.

Gustin, M. C., X. L. Zhou, B. Martinac, and C. Kung. 1988. A mechanosensitive ion channel in the yeast plasma membrane. *Science.* 242:762–765.

Hamill, O. P., and B. Martinac. 2001. Molecular basis of mechanotransduction in living cells. *Physiol. Rev.* 81:685–740.

Hamill, O. P., and D. W. McBride, Jr. 1992. Rapid adaptation of single mechanosensitive channels in *Xenopus* oocytes. *Proc. Natl. Acad. Sci. USA.* 89:7462–7466.

Hase, C. C., A. C. Le Dain, and B. Martinac. 1995. Purification and functional reconstitution of the recombinant large mechanosensitive ion channel (MscL) of *Escherichia coli*. *J. Biol. Chem.* 270:18329–18334.

Ingber, D. E. 1993. Cellular tensegrity: defining new rules of biological design that govern the cytoskeleton. *J. Cell Sci.* 104:613–627.

Johnson, K. L. 1985. Contact Mechanics. Cambridge University Press, Cambridge.

Jones, W. R., H. P. Ting-Beall, G. M. Lee, S. S. Kelley, R. M. Hochmuth, and F. Guilak. 1999. Alterations in the Young's modulus and volumetric properties of chondrocytes isolated from normal and osteoarthritic human cartilage. *J. Biomech.* 32:119–127.

Kanzaki, M., M. Nagasawa, I. Kojima, C. Sato, K. Naruse, M. Sokabe, and H. Iida. 1999. Molecular identification of a eukaryotic, stretch-activated nonselective cation channel. *Science.* 285:882–886.

Kirber, M. T., A. Guerrero-Hernandez, D. S. Bowman, K. E. Fogarty, R. A. Tuft, J. J. Singer, and F. S. Fay. 2000. Multiple pathways responsible for the stretch-induced increase in Ca2+ concentration in toad stomach smooth muscle cells. *J. Physiol.* 524:3–17.

Ko, K. S., and C. A. McCulloch. 2000. Partners in protection: interdependence of cytoskeleton and plasma membrane in adaptations to applied forces. *J. Membr. Biol.* 174:85–95.

Lee, J. C., D. T. Wong, and D. E. Discher. 1999. Direct measures of large, anisotropic strains in deformation of the erythrocyte cytoskeleton. *Biophys. J.* 77:853–864.

Lehenkari, P., G. T. Charras. S. A. Nesbitt, and M. A. Horton. 1999. New technologies in scanning probe microscopy for the understanding of molecular interactions in cells. *In* Expert Reviews in Molecular Medicine @ www-ermm.cbcu.cam.ac.uk.

Lehenkari, P. P., G. T. Charras, A. Nykanen, and M. A. Horton. 2000. Adapting atomic force microscopy for cell biology. *Ultramicroscopy.* 82:289–95.

Maniotis, A. J., C. S. Chen, and D. E. Ingber. 1997. Demonstration of mechanical connections between integrins, cytoskeletal filaments, and nucleoplasm that stabilize nuclear structure. *Proc. Natl. Acad. Sci. USA.* 94:849–854.

McNeil, P. L., S. S. Vogel, K. Miyake, and M. Terasaki. 2000. Patching plasma membrane disruptions with cytoplasmic membrane. *J. Cell Sci.* 113:1891–1902.

Merkel, R., R. Simson, D. A. Simson, M. Hohenadl, A. Boulbitch, E. Wallraff, and E. Sackmann. 2000. A micromechanic study of cell polarity and plasma membrane cell body coupling in *Dictyostelium*. *Biophys. J.* 79:707–719.

Mills, L. R., and C. E. Morris. 1998. Neuronal plasma membrane dynamics evoked by osmomechanical perturbations. *J. Membr. Biol.* 166:223–235.

Oghalai, J. S., A. A. Patel, T. Nakagawa, and W. E. Brownell. 1998. Fluorescence-imaged microdeformation of the outer hair cell lateral wall. *J. Neurosci.* 18:48–58.

Opsahl, L. R., and W. W. Webb. 1994. Lipid-glass adhesion in giga-sealed patch-clamped membranes. *Biophys. J.* 66:75–79.

Radmacher, M. 1997. Measuring the elastic properties of biological samples with the AFM. *IEEE Eng. Med. Biol. Mag.* 16:47–57.

Raucher, D., and M. P. Sheetz. 1999. Characteristics of a membrane reservoir buffering membrane tension. *Biophys. J.* 77:1992–2002.

Rubin, C. T., and L. E. Lanyon. 1984. Regulation of bone formation by applied dynamic loads. *J. Bone Joint Surg. Am.* 66:397–402.

Sachs, F., and C. E. Morris. 1998. Mechanosensitive ion channels in nonspecialized cells. *Rev. Physiol. Biochem. Pharmacol.* 132:1–77.

Sakmann, B., and E. Neher. 1995. Geometric parameters of pipettes and membrane patches. *In* Single Channel Recording. B. Sakmann and E. Neher, editors. Plenum Press, New York. 637–650.

Sokabe, M., F. Sachs, and Z. Q. Jing. 1991. Quantitative video microscopy of patch clamped membranes stress, strain, capacitance, and stretch channel activation. *Biophys. J.* 59:722–728.

Sukharev, S., M. Betanzos, C. S. Chiang, and H. R. Guy. 2001. The gating mechanism of the large mechanosensitive channel MscL. *Nature*. 409:720–724.

Sukharev, S. I., W. J. Sigurdson, C. Kung, and F. Sachs. 1999. Energetic and spatial parameters for gating of the bacterial large conductance mechanosensitive channel, MscL. *J. Gen. Physiol.* 113:525–540.

Theret, D. P., M. J. Levesque, M. Sato, R. M. Nerem, and L. T. Wheeler. 1988. The application of a homogeneous half-space model in the analysis of endothelial cell micropipette measurements. *J. Biomech. Eng.* 110:190–199.

Thoumine, O., O. Cardoso, and J. J. Meister. 1999. Changes in the mechanical properties of fibroblasts during spreading: a micromanipulation study. *Eur. Biophys. J.* 28:222–234.

Timoshenko, S. P., and J. N. Goodier. 1970. Theory of Elasticity. McGraw-Hill, New York.

Tseng, Y., and D. Wirtz. 2001. Mechanics and multiple-particle tracking microheterogeneity of alpha-actinin-cross-linked actin filament networks. *Biophys. J.* 81:1643–1656.

Wan, X., P. Juranka, and C. E. Morris. 1999. Activation of mechanosensitive currents in traumatized membrane. *Am. J. Physiol.* 276:C318–C327.

Wang, N., K. Naruse, D. Stamenovic, J. J. Fredberg, S. M. Mijailovich, I. M. Tolic-Norrelykke, T. Polte, R. Mannix, and D. E. Ingber. 2001. Mechanical behavior in living cells consistent with the tensegrity model. *Proc. Natl. Acad. Sci. USA*. 98:7765–7770.

Wu, H. W., T. Kuhn, and V. T. Moy. 1998. Mechanical properties of L929 cells measured by atomic force microscopy: effects of anticytoskeletal drugs and membrane crosslinking. *Scanning*. 20:389–397.

Zhu, C., G. Bao, and N. Wang. 2000. Cell mechanics: mechanical response, cell adhesion, and molecular deformation. *Annu. Rev. Biomed. Eng.* 2:189–226.

Zou, H., L. M. Lifshitz, R. A. Tuft, K. E. Fogarty, and J. J. Singer. 2002. Visualization of Ca2+ entry through single stretch-activated cation channels. *Proc. Natl. Acad. Sci. USA*. 99:6404–6409.